Development of a Ring-type Flywheel Battery System for Storage of Renewable Energy

Chow-Shing Toh
Advanced Institute of Manufacturing with High-tech Innovations, National Chung Cheng University
Chiayi, Taiwan

Shyh-Leh Chen*
Advanced Institute of Manufacturing with High-tech Innovations, National Chung Cheng University
Chiayi, Taiwan

Dar-Ping Juang
Chung-Shan Institute of Science & Technology
Taoyuan, Taiwan

Abstract

In this study, a small scale prototype of a ring-type flywheel battery system is designed and fabricated. The system consists of 5-DOF magnetic bearing and a built-in motor/generator. The magnetic bearing is of hybrid type, with passive axial magnetic bearing and active radial magnetic bearing. For the passive axial magnetic bearing, a pair of Halbach arrays of permanent magnets are arranged vertically to support the weight of rotor and flywheel. For the active radial magnetic bearing, a set of Halbach array is placed on the rotor side, which will correspond to a coil set on the stator side. The active magnetic bearing can produce both attraction and repulsion forces on the radial direction, depending on the direction of the coil currents. When driven by an active feedback control system operating in conjunction with a position sensor, the actuator force can be used to balance the lateral forces coupled from the passive axial magnetic bearing and to achieve stable levitation. In the radial magnetic bearing, the design of eight-pole and differential winding mode are applied, which can result in a linear force-current relation. Hence, the system can be modeled by a simple linear time-invariant system. For robustness, the controller is designed by integral sliding mode control (ISMC) to overcome the effects of uncertainty and to achieve good steady-state accuracy. Numerical simulation results verify the effectiveness of the controller. To further validate the efficiency of the proposed controller, the experiments of the prototype are also performed.

1 Introduction

Several hundred years ago pure mechanical flywheels where used solely to keep machines running smoothly from cycle to cycle, thereby render possible the industrial revolution. During that time several shapes and designs where implemented, but it took until the early 20th century before flywheel rotor shapes and rotational stress were thoroughly analyzed. Later in the 1970s flywheel energy storage was proposed as a primary objective for electric vehicles and stationary power backup. At the time fiber composite rotors where built, and in the 1980s magnetic bearings started to appear. Thus the potential for using flywheels as electric energy storage has long been established by extensive research.

More recent improvements in material, magnetic bearings and power electronics make flywheels a competitive choice for a number of energy storage applications. First generation flywheel mainly is made by material such as steel, but have low energy storage density. Second generation flywheels of composite materials have higher energy storage density but limited mass due to structural and stability limitations [1, 2]. The third generation flywheels – "Power Rings" - using radial magnetic bearings to levitate thin-walled composite hoops rotated at high speed to store kinetic energy with power density greater than that of chemical batteries [3].

The ability of flywheel systems to quickly charge and discharge is a key technology for applications requiring pulse power. Moreover, High speed is desirable since the energy stored is proportional to the square of the speed but only linearly proportional to the mass. Hence, magnetic bearings represent a preferred alternative to conventional mechanical bearing designs in this application. Because magnetic bearing enables to support rotor without friction and it also provides low internal losses during long-term storage. Decoupling control approach has been developed for a nonlinear system with a rotor of five degree-of-freedom supported by two radial magnetic bearings [4]. Nonlinear controllers based on dynamic feedback linearization are designed such that the strongly coupled rotor

*Contact Author Information: imeslc@ccu.edu.tw, 168 University Road, Minhsiung Township, Chiayi County 62102, Taiwan, ROC, Phone:+886-5-272-0411 ext 33320, Fax:+886-5-272-0589

motion is reduced to five decoupled normalization linear subsystems including four rotor displacements and its speed, the PID controller [5] and sliding mode control [6] was introduced. The advantage of eight-pole radial bearings is the fact that two pole pairs each can be assigned to Cartesian coordinates *x* and *y* which are often used in mechanics [7]. Simulation of the mechanical system, control design, and measurement of the rotor motion are usually based on these coordinates, simplifying bearing control.

Passive magnetic bearings have several advantages, such as they require no input energy and no power for cooling. To the passive magnetic bearings, the simplest type is composed of two monolithic permanent magnetic rings with either axial magnetization or radial magnetization, and a special design of passive magnetic bearing is proposed to overcome radial and axial loads in both directions [8]. This shear-force levitator is laterally unstable and must be actively stabilized by the attraction and repulsion which provided by active magnetic bearings [9].

Fortunately, with the particular design and winding scheme of active magnetic bearings, it produces a linear force-current relation in neighbourhood of equilibrium point, so that the plant can be simplified as linear time-invariant system. In controller design, Integral Sliding Mode Control (ISMC) are applied to overcome the effect of uncertainty, and to achieve good steady-state accuracy.

2 System Modeling

2.1 Description of the Flywheel System

Figure 1 is the ring-type flywheel battery prototype which studied in this paper, and the configuration is mainly follows the one proposed in [2]. The system consists of 5-DOF magnetic bearing and a built-in motor/generator, and the magnetic bearing is of hybrid type, including passive axial magnetic bearing and active radial magnetic bearing. For the passive axial magnetic bearing, a pair of Halbach arrays of permanent magnetic rings are arranged vertically to support the weight of rotor and flywheel. For the active radial magnetic bearing, a set of Halbach array is placed on the rotor side, which will correspond to 8 coil sets on the stator side. The active magnetic bearing can produce both attraction and repulsion forces on the radial direction, depending on the direction of the coil currents. When driven by an active feedback control system operating in conjunction with a position sensor, the actuator force can be used to balance the lateral forces coupled from the passive axial magnetic bearing and to achieve stable levitation.

The motor/generator is installed at the center of the flywheel battery system. When it is acting as a motor, electric energy supplied to the stator winding, causing the rotor to spin and to gain rotational energy. In generator mode, the rotational energy stored in the rotor can be extracted by power electronics circuit and is converted to electric energy as output.

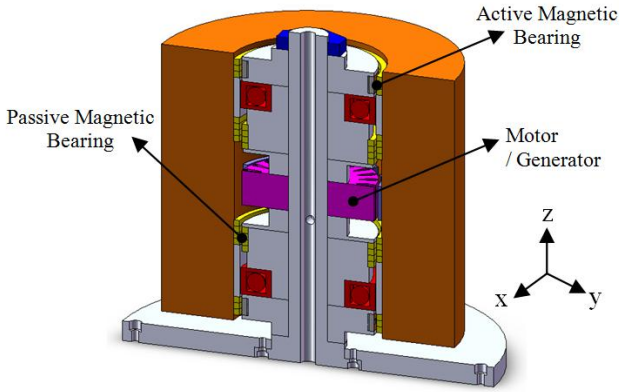

Figure 1: The configuration of proposed prototype flywheel battery system

2.2 Magnetic Bearing

The configuration of the stabilization actuator or the so-called active magnetic bearings is shown in Figure 2. As mentioned previously, the passive magnetic bearings are laterally unstable and must be actively stabilized by the attraction and repulsion provided by the AMB. Positive current will cause attractive force on the moving array, and negative current provides repulsion. Vertical forces produced by the upper and lower sides of the coil are equal and

opposite, and so no net vertical force is applied to the moving array. In order to identify the relationship between magnetic force, pole area, coil current, and air gap, we made some measurement with several sizes of permanent magnet, coil turns, and pole area. Finally, experimental measurement indicates that for each DOF, the magnetic force of the AMB is linearly proportional to the coil current and can be approximated as Equation (1), as well the data is shown in Figure 3.

$$f \approx \left(\frac{k_{a1}}{s^3} + \frac{k_{a2}}{s^2} + \frac{k_{a3}}{s} + k_{a4} \right) i \tag{1}$$

where s is air gap, i is coil current, and k_{a1}, k_{a2}, k_{a3} are constant coefficient in terms of pole area and coil turns. Note that positive f denotes repulsion and negative denotes attraction of function.

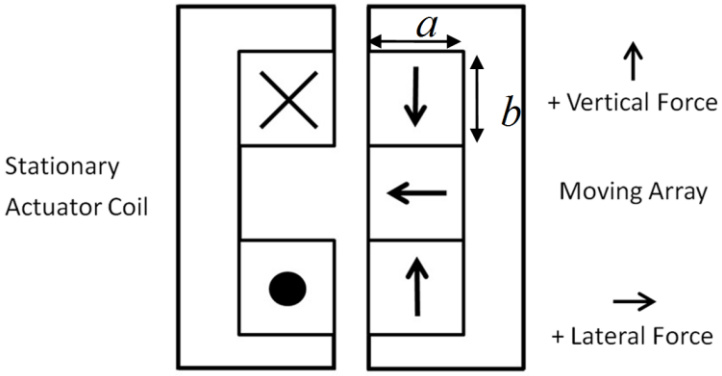

Figure 2: The configuration of active magnetic bearing

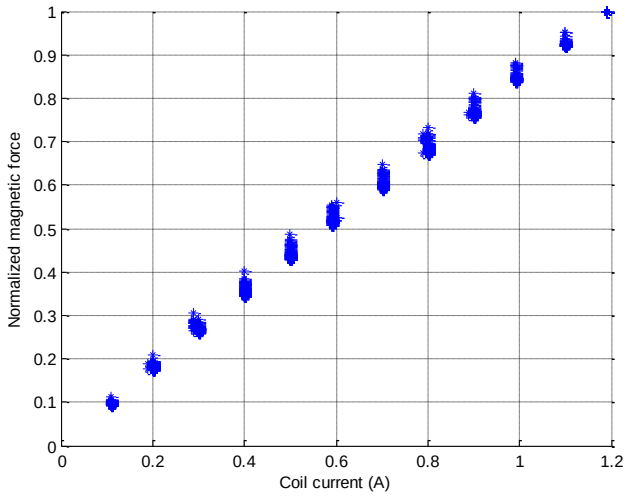

Figure 3: The experimental measurement data

In the present system, the winding scheme of the AMB is shown in Figure 4. There are 8 coil sets on the stator (inner part). The opposite coil sets (apart by 180 degrees) are wired in a differential way. As a result, there are four independent control currents in this system, and bias currents are not necessary. In other words, the magnetic force at the 4 DOFs can be approximated as

$$f_{atx} \approx k_1 i_{tx} \ , \ f_{aty} \approx k_2 i_{ty} \tag{2}$$

$$f_{abx} \approx k_3 i_{bx} \ , \ f_{aby} \approx k_4 i_{by} \tag{3}$$

where $i_{tx}, i_{ty}, i_{bx}, i_{by}$ are control currents and k_1, k_2, k_3, k_4 are constant. The subscript with "a" denotes active magnetic bearing and subscript with "t" and "b" denotes top and bottom active magnetic bearing.

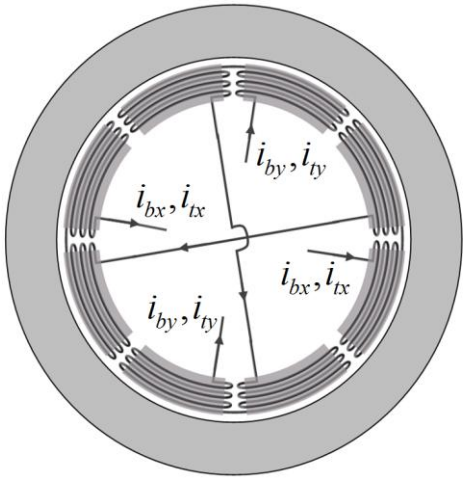

Figure 4: The winding scheme of active magnetic bearing

Next, the sectional view and configuration of the passive magnetic bearing are shown in Figure 5 and it is consists of 4 layer of ring-type permanent magnet and apply Halbach array. Actually, our strategic is try to understand the magnetic force model from a variety of material and dimension of permanent magnet through experimental measurement, as well the shape of permanent magnet are cuboid at initial stage. From Figure 6, we can know that the operating point must be located at positive side to overcome mass of moving array and rotor, so that the passive magnetic bearing provide lateral magnetic force simultaneously. Similary, a approximation of magnetic force came out from the experimental data, and it can be expressed as

$$f \approx \frac{\tilde{k}_1(z)}{s^2} + \frac{\tilde{k}_2(z)}{s} + \tilde{k}_3(z) \tag{4}$$

where

$$\tilde{k}_i(z) = \hat{k}_n z^n + \hat{k}_{n-1} z^{n-1} + \cdots + \hat{k}_1 z + \hat{k}_0 \quad , i = 1,2,3 \tag{5}$$

where z is offset and $\hat{k}_j$ are constant.

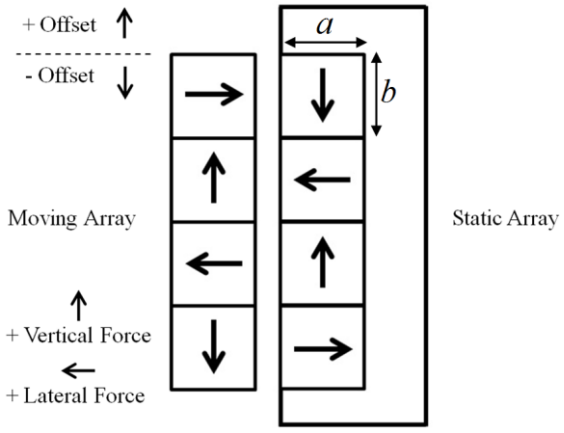

Figure 5: The configuration of passive magnetic bearing

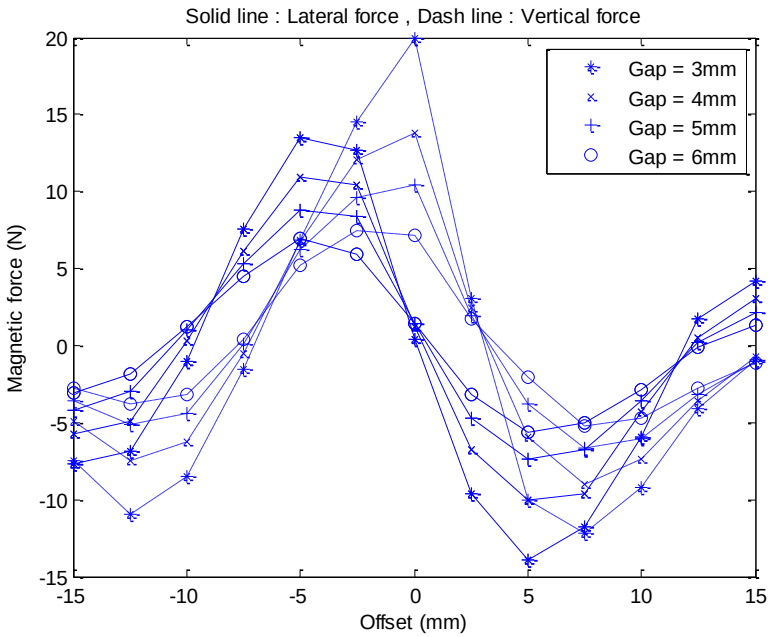

Figure 6: The behavior of magnetic force for 5mm x 5mm x 30mm magnets

The passive magnetic bearings consist of permanent magnet segments of equal sizes on the inner wall of rotor and outer wall of stator. Since the permanent magnets are arranged in a symmetric way, when the rotor is running at the steady state equilibrium point, the summation force at the radial directions will be zero. In order to linearize the magnetic force, we consider that ring-type permanent magnet are consists of a lot of cuboid permanent magnet, so the magnetic force provided by the passive magnetic bearings at the 4 DOFs can be approximated as Equation (6)~(7). By the way, because of the wall of ring-type magnets are quite thin and the diameters are large for this prototype, the ring-type magnets are hard to fabricated and magnetization, so the passive magnetic bearings are consists of segmented arc-shaped permanent magnets at fact.

$$f_{ptx} \approx k_5\, x_t + k_6\, x_b \ , \ \ f_{pty} \approx k_7\, y_t + k_8\, y_b \tag{6}$$

$$f_{pbx} \approx k_9\, x_t + k_{10}\, x_b \ , \ \ f_{pby} \approx k_{11}\, y_t + k_{12}\, y_b \tag{7}$$

The subscript with "p" denotes passive magnetic bearing. Where x_t, x_b, y_t, y_b is displacement of rotor which located on magnetic bearing, and $k_5, k_6, k_7, k_8, k_9, k_{10}, k_{11}, k_{12}$ are constant.

2.3 Governing Equation

In order to obtain the equation of motions for this flywheel battery prototype, Newton's Second Law is applied here. The total moments and forces can be expressed as

$$\sum F_x = k_1\, i_{tx} + k_3\, i_{bx} + k_{13}\, x_t + k_{14}\, x_b \tag{8}$$

$$\sum F_y = k_2\, i_{ty} + k_4\, i_{by} + k_{15}\, y_t + k_{16}\, y_b \tag{9}$$

$$\sum M_x = k_4\, i_{by}\, l_b - k_2\, i_{ty}\, l_t + k_{17}\, y_t + k_{18}\, y_b \tag{10}$$

$$\sum M_y = k_1 i_{tx} l_t - k_3 i_{bx} l_b + k_{19} x_t + k_{20} x_b \tag{11}$$

where

$$k_{13} = k_5 + k_9 \text{ , } k_{14} = k_6 + k_{10} \tag{12}$$

$$k_{15} = k_7 + k_{11} \text{ , } k_{16} = k_8 + k_{12} \tag{13}$$

$$k_{17} = k_{11} l_{bp} - k_7 l_{tp} \text{ , } k_{18} = k_{12} l_{bp} - k_8 l_{tp} \tag{14}$$

$$k_{19} = k_5 l_{tp} - k_9 l_{bp} \text{ , } k_{20} = k_6 l_{tp} - k_{10} l_{bp} \tag{15}$$

It is assumed that the rotating speed is constant ($\dot{\omega} = 0$) and the rotor displacement at z -direction is very small, and the derivations for angular momentum and acceleration of center of mass in terms of displacements and velocity of rotor at AMBs are neglected here. Then, the equations of motion can be obtained by Newton's law and expressed as

$$\sum F_x = m \frac{l_t \ddot{x}_b + l_b \ddot{x}_t}{l_t + l_b} \tag{16}$$

$$\sum F_y = m \frac{l_t \ddot{y}_b + l_b \ddot{y}_t}{l_t + l_b} \tag{17}$$

$$\sum M_x = I \frac{\ddot{y}_t - \ddot{y}_b}{l_b + l_t} + I_z \omega \frac{\dot{x}_b - \dot{x}_t}{l_b + l_t} \tag{18}$$

$$\sum M_y = I \frac{\ddot{x}_b - \ddot{x}_t}{l_b + l_t} - I_z \omega \frac{\dot{y}_t - \dot{y}_b}{l_b + l_t} \tag{19}$$

The superscript "$\cdot$" denotes differentiation with respect to time. Note that l_b , l_t is distance between center of gravity and active magnetic bearing, l_{bp}, l_{tp} is distance between center of gravity and passive magnetic bearing and m is mass of rotor. Also, cross-section radial and polar mass moment of inertia are indicated as I and I_z , and ω is rotating speed.

3 Controller Design

3.1 State Space Model

With the arrival of space exploration, requirements for control systems increased in scope. Modeling systems by linear, time-invariant differential equations and subsequent transfer functions became inadequate. The state-space, approach (also referred to as the modern, or time-domain, approach) is a unified method for modeling, analyzing, and designing a wide range of systems. Many systems do not have just a single input and a single output. Multiple-input, multiple-output systems can be compactly represented in state space with a model similar in form and complexity to that used for single-input, single-output systems. The state-space approach is also attractive because of the availability of numerous state-space software packages for the personal computer. Hence, from equations of motion (16)-(19), the state space representation for this model can be expressed as

$$\dot{x} = \mathbf{A}\,x + \mathbf{B}u = \begin{bmatrix} \mathbf{A}_{11} & \mathbf{A}_{12} \\ \mathbf{A}_{21} & \mathbf{A}_{22} \end{bmatrix} x + \begin{bmatrix} \mathbf{B}_{11} \\ \mathbf{B}_{21} \end{bmatrix} u \tag{20}$$

where

$$x = \begin{Bmatrix} x_1 & x_2 & x_3 & x_4 & x_5 & x_6 & x_7 & x_8 \end{Bmatrix}^T \tag{21}$$

$$x_1 = x_b \ , \ x_2 = \dot{x}_b \ , \ x_3 = y_b \ , \ x_4 = \dot{y}_b \tag{22}$$

$$x_5 = x_t \ , \ x_6 = \dot{x}_t \ , \ x_7 = y_t \ , \ x_8 = \dot{y}_t \tag{23}$$

$$u = \begin{Bmatrix} i_{bx} & i_{by} & i_{tx} & i_{ty} \end{Bmatrix}^T \tag{24}$$

$$\mathbf{A}_{11} = \begin{bmatrix} 0 & 1 & 0 & 0 \\ \frac{k_{14}}{m} + \frac{l_b k_{20}}{I} & 0 & 0 & -\frac{l_b I_z \omega}{(l_b + l_t) I} \\ 0 & 0 & 0 & 1 \\ 0 & \frac{l_b I_z \omega}{(l_b + l_t) I} & \frac{k_{16}}{m} - \frac{l_b k_{18}}{I} & 0 \end{bmatrix} \tag{25}$$

$$\mathbf{A}_{12} = \begin{bmatrix} 0 & 0 & 0 & 0 \\ \frac{k_{13}}{m} + \frac{l_b k_{19}}{I} & 0 & 0 & \frac{l_b I_z \omega}{(l_b + l_t) I} \\ 0 & 0 & 0 & 0 \\ 0 & -\frac{l_b I_z \omega}{(l_b + l_t) I} & \frac{k_{15}}{m} - \frac{l_b k_{17}}{I} & 0 \end{bmatrix} \tag{26}$$

$$\mathbf{A}_{21} = \begin{bmatrix} 0 & 0 & 0 & 0 \\ \frac{k_{14}}{m} - \frac{l_t k_{20}}{I} & 0 & 0 & \frac{l_t I_z \omega}{(l_b + l_t) I} \\ 0 & 0 & 0 & 0 \\ 0 & -\frac{l_t I_z \omega}{(l_b + l_t) I} & \frac{k_{16}}{m} + \frac{l_t k_{18}}{I} & 0 \end{bmatrix} \tag{27}$$

$$\mathbf{A}_{22} = \begin{bmatrix} 0 & 1 & 0 & 0 \\ \frac{k_{13}}{m} - \frac{l_t k_{19}}{I} & 0 & 0 & -\frac{l_t I_z \omega}{(l_b + l_t) I} \\ 0 & 0 & 0 & 1 \\ 0 & \frac{l_t I_z \omega}{(l_b + l_t) I} & \frac{k_{15}}{m} + \frac{l_t k_{17}}{I} & 0 \end{bmatrix} \tag{28}$$

$$\mathbf{B}_{11} = \begin{bmatrix} 0 & 0 & 0 & 0 \\ \frac{k_3}{m} - \frac{k_3 l_b^2}{I} & 0 & \frac{k_1}{m} + \frac{k_1 l_b l_t}{I} & 0 \\ 0 & 0 & 0 & 0 \\ 0 & \frac{k_4}{m} - \frac{k_4 l_b^2}{I} & 0 & \frac{k_2}{m} + \frac{k_2 l_b l_t}{I} \end{bmatrix} \tag{29}$$

$$\mathbf{B}_{21} = \begin{bmatrix} 0 & 0 & 0 & 0 \\ \frac{k_3}{m} + \frac{k_3 l_t l_b}{I} & 0 & \frac{k_1}{m} - \frac{k_1 l_t^2}{I} & 0 \\ 0 & 0 & 0 & 0 \\ 0 & \frac{k_4}{m} + \frac{k_4 l_t l_b}{I} & 0 & \frac{k_2}{m} - \frac{k_2 l_t^2}{I} \end{bmatrix} \tag{30}$$

3.2 Robust Control (I.S.M.C)

The mathematical model is based on perfect models, which are almost impossible to exist in practice. A more reasonable assumption is that real system model is nominal one plus a bounded uncertain part $\Delta f(x,\phi(x,u))$. In what follows, quantities of the nominal system are represented with an "$\frown$", the Equation (20) can becomes

$$\dot{x} = \overset{\frown}{f}(x,\phi(x,u)) + \Delta f(x,\phi(x,u)) \tag{31}$$

Lyapunov-based control methods such as Lyapunov redesign, sliding mode control, adaptive control, etc, can be used to achieve robust stabilization. In this paper, an integral sliding mode controller will be designed to allow for large uncertainties and to achieve good steady-state accuracy. To facilitate the controller design, Equation (31) is rewritten in the regular form as

$$\dot{\eta} = \xi \tag{32}$$

$$\dot{\xi} = \overset{\frown}{f}_a(\eta,\xi) + \mathbf{G}_{\mathrm{B}}\left[u + \delta_{\xi}(\eta,\xi,u)\right] \tag{33}$$

where

$$\eta = \begin{Bmatrix} x_1 & x_3 & x_5 & x_7 \end{Bmatrix}^T \tag{34}$$

$$\xi = \begin{Bmatrix} x_2 & x_4 & x_6 & x_8 \end{Bmatrix}^T \tag{35}$$

$$\mathbf{G}_{\mathrm{B}} = \begin{bmatrix} \frac{k_3}{m} - \frac{k_3 l_b^2}{I} & 0 & \frac{k_1}{m} + \frac{k_1 l_b l_t}{I} & 0 \\ 0 & \frac{k_4}{m} - \frac{k_4 l_b^2}{I} & 0 & \frac{k_2}{m} + \frac{k_2 l_b l_t}{I} \\ \frac{k_3}{m} + \frac{k_3 l_t l_b}{I} & 0 & \frac{k_1}{m} - \frac{k_1 l_t^2}{I} & 0 \\ 0 & \frac{k_4}{m} + \frac{k_4 l_t l_b}{I} & 0 & \frac{k_2}{m} - \frac{k_2 l_t^2}{I} \end{bmatrix} \tag{36}$$

where $\eta \in IR^{n-p}$, $\xi \in IR^p$, $u \in IR^p$, and $\delta_{\xi}(\eta,\xi,u)$ is unknown smooth functions of η, ξ and u, representing uncertainties or disturbances. It is obvious that the uncertainty $\delta_{\xi}(\eta,\xi,u)$ satisfies the matching condition. Assume that $\mathbf{G}_{\mathrm{B}}$ is nonsingular in the domain of interest and invertible. The integral sliding mode control takes an integral sliding manifold

$$\sigma = \xi + b_1\eta + b_2 x_m \ , \ \dot{x}_m = \eta \tag{37}$$

where b_1 and b_2 are positive constants. The strategy of integral sliding mode control is only required to maintain $\dot{\sigma} = 0$ (or $\sigma =$ constant). Therefore, η and hence ξ will approach zero asymptotically. To this aim, the control input u consists of equivalent control u_{eq} and switching control u_s.

$$u = u_{eq} + u_s \tag{38}$$

The equivalent control u_{eq} is to maintain the condition $\dot{\sigma} = 0$, in the absence of uncertainty, and obtained as

$$u_{eq} = \mathbf{G}_{\mathrm{B}}{}^{-1}\left(-\mathbf{G}_{\mathrm{A}}x - b_1\xi - b_2\eta\right) \tag{39}$$

where

$$\mathbf{G}_{\mathrm{A}} = \begin{bmatrix} \mathbf{G}_{\mathrm{A1}} & \mathbf{G}_{\mathrm{A2}} \end{bmatrix} \tag{40}$$

$$\mathbf{G}_{\mathrm{A1}} = \begin{bmatrix} \frac{k_{14}}{m} + \frac{l_b k_{20}}{I} & 0 & 0 & -\frac{l_b I_z \omega}{(l_b + l_t) I} \\ 0 & \frac{l_b I_z \omega}{(l_b + l_t) I} & \frac{k_{16}}{m} - \frac{l_b k_{18}}{I} & 0 \\ \frac{k_{14}}{m} - \frac{l_t k_{20}}{I} & 0 & 0 & \frac{l_t I_z \omega}{(l_b + l_t) I} \\ 0 & -\frac{l_t I_z \omega}{(l_b + l_t) I} & \frac{k_{16}}{m} + \frac{l_t k_{18}}{I} & 0 \end{bmatrix} \tag{41}$$

$$\mathbf{G}_{\mathrm{A2}} = \begin{bmatrix} \frac{k_{13}}{m} + \frac{l_b k_{19}}{I} & 0 & 0 & \frac{l_b I_z \omega}{(l_b + l_t) I} \\ 0 & -\frac{l_b I_z \omega}{(l_b + l_t) I} & \frac{k_{15}}{m} - \frac{l_b k_{17}}{I} & 0 \\ \frac{k_{13}}{m} - \frac{l_t k_{19}}{I} & 0 & 0 & -\frac{l_t I_z \omega}{(l_b + l_t) I} \\ 0 & \frac{l_t I_z \omega}{(l_b + l_t) I} & \frac{k_{15}}{m} + \frac{l_t k_{17}}{I} & 0 \end{bmatrix} \tag{42}$$

When the system states are not on the sliding manifold initially, the switching control u_s is applied to force them reaching $\dot{\sigma} = 0$ in finite time. Bringing back the uncertainties and $\dot{\sigma}$ become

$$\dot{\sigma} = \mathbf{G}_{\mathrm{B}} u_s + \mathbf{G}_{\mathrm{B}} \delta_{\xi}(\eta, \xi, u_s + u_{eq}) \tag{43}$$

where $\mathbf{G}_{\mathrm{B}} \delta_{\xi}(\eta, \xi, u_s + u_{eq}) = \Delta(\eta, \xi, u)$. Suppose that within the AMB's operational domain, an upper bound on the uncertainty $\Delta(\eta, \xi, u)$ is known

$$\left\| \Delta(\eta, \xi, u) \right\|_{\infty} \le \rho + k_c \left\| u \right\|_{\infty} \tag{44}$$

where $\rho \ge 0$ amounts to the estimate on the open loop uncertainty. It is not restricted to be small here. On the other hand, $0 \le k_c < 1$ represents the bound on control-related uncertainty. It cannot exceed the magnitude of the real control to prevent from losing control authority. With the uncertainty bounds given by Equation (44) and utilizing Lyapunov function candidates $V_j = \frac{1}{2}\sigma_j^2$ for $j = 1 \sim 4$, we can obtain

$$\dot{V}_j = \sigma_j \dot{\sigma}_j \le \sigma_j [\mathbf{G}_{\mathrm{B}} u_s + \mathbf{G}_{\mathrm{B}} \delta_{\xi}(\eta, \xi, u_s + u_{eq})] \tag{45}$$

and the switching control can be designed as

$$u_s = -\mathbf{G}_{\mathrm{B}}^{-1} \left(\frac{\rho + \alpha}{1 - k_c} \right) \tanh(\sigma_j, \varepsilon) \tag{46}$$

where

$$\tanh(\sigma_j,\varepsilon)=\left\{\tanh(\frac{\sigma_1}{\varepsilon}) \quad \tanh(\frac{\sigma_2}{\varepsilon}) \quad \tanh(\frac{\sigma_3}{\varepsilon}) \quad \tanh(\frac{\sigma_4}{\varepsilon})\right\}^T \tag{47}$$

Note that α and ε are positive constants, and $sat(\sigma_j/\varepsilon)$ is the saturation function. Finally, yielding a overall closed-loop system as

$$\dot{x}_m=\eta \tag{48}$$

$$\dot{x} = \mathbf{A}x+\mathbf{B}\mathbf{G}_{\mathrm{B}}^{-1}\left(\mathbf{G}_{\mathrm{A}}x-b_1\xi-b_2\eta-\left(\frac{\rho+\alpha}{1-k_c}\right)sat\left(\frac{\sigma_1}{\varepsilon}\right)\right) \tag{49}$$

4 Simulations

For all simulations in this section, the system parameters and geometric sizes are given in Table 1, and the detailed information of magnetic bearings is listed in Table 2. We consider that operating speed is 10000 rpm and it will be start to rotate at t=0.2s, as well the dynamic of motor will be neglected through MATLAB SIMULINK.

Mass of Rotor, m	12.605kg
Rotating speed, ω	10000 rpm
Diametral mass moment of inertia , I	$0.101925\mathrm{kgm}^2$
Polar mass moment of inertia , I_z	$0.104311\mathrm{kgm}^2$
Distance between center of gravity and bottom active magnetic bearing, l_b	$9.525\times10^{-2}\mathrm{m}$
Distance between center of gravity and top active magnetic bearing, l_t	$9.875\times10^{-2}\mathrm{m}$
Distance between center of gravity and bottom active magnetic bearing, l_{bp}	$3.874\times10^{-2}\mathrm{m}$
Distance between center of gravity and top active magnetic bearing, l_{tp}	$4.523\times10^{-2}\mathrm{m}$

Table 1: Parameters of proposed flywheel battery prototype

Nominal air gap of AMB	$2\times10^{-4}\mathrm{m}$
Nominal air gap of PMB	$2.5\times10^{-4}\mathrm{m}$
Cross section of magnetic pole	$1.24\times10^{-3}\mathrm{m}^2$
Number of coil turns	270
Width of permanent magnet, a	$5\times10^{-3}\mathrm{m}$
Height of permanent magnet, b	$5\times10^{-3}\mathrm{m}$

Table 2: Parameters of active and passive magnetic bearing

The initial states of simulation case are $x(0)=[-3.53\text{x}10^{-4}\text{m}\ 0\ 3.53\text{x}10^{-4}\text{m}\ 0\ 3.53\text{x}10^{-4}\text{m}\ 0\ -3.53\text{x}10^{-4}\text{m}]^T$. Note that two additional states are needed for ISMC, which are taken to be $x_m(0)=[0,0]^T$. The initial states for ISMC are thus $[x_m(0), x(0)]^T$. Moreover, the parameters of I.S.M.C controller are listed on Table 3, mainly provided by trial and error. The results of numerical simulation are shown in Figure 6~11, including trajectory of rotor on the magnetic bearings, displacements of rotor at AMBs, and the control current i_{bx}, i_{by}, i_{tx}, i_{ty}.

b_1	b_2	ρ_c	α	k_c	ε
50	150	5	2	0.7	0.5

Table 3: Parameters of Integral Sliding Mode Controller

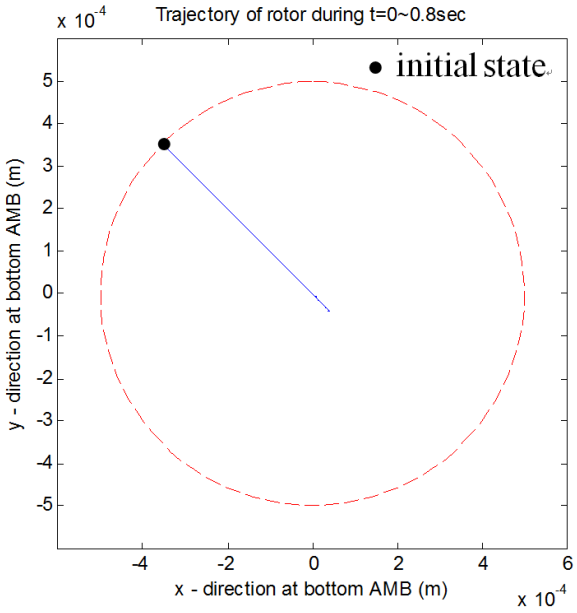

Figure 7: Trajectory of rotor at bottom active magnetic bearing

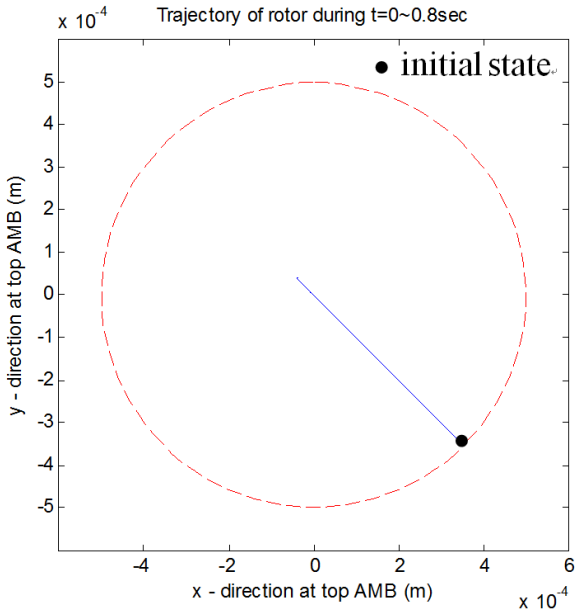

Figure 8: Trajectory of rotor at top active magnetic bearing

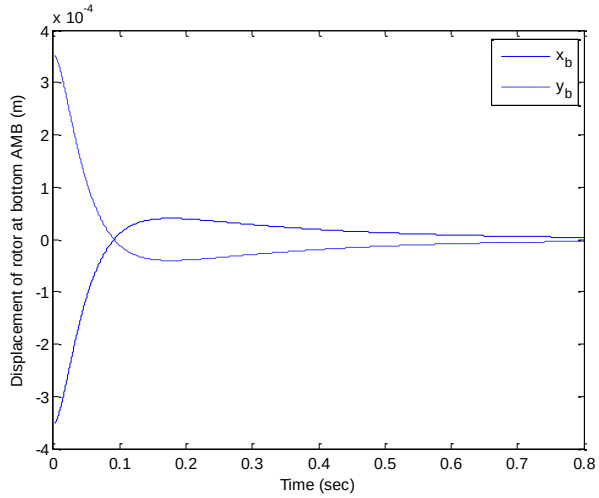

Figure 9: Displacements of rotor at bottom active magnetic bearing

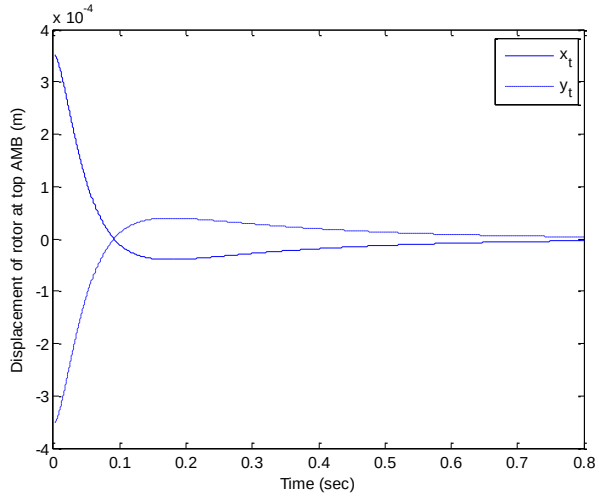

Figure 10: Displacements of rotor at top active magnetic bearing

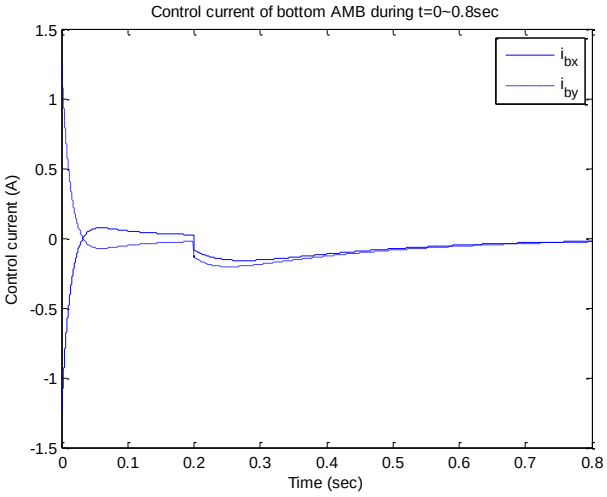

Figure 11: Control current for i_{bx}, i_{by}

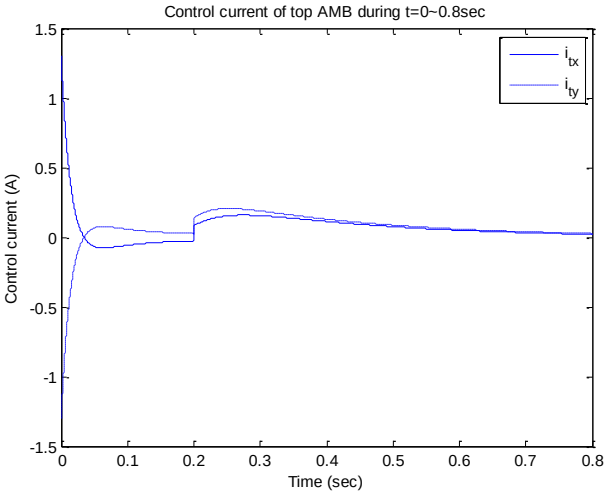

Figure 12: Control current for i_{tx}, i_{ty}

With the above control parameters, the initial control currents of the I.S.M.C controller all lie in the range (–3A, 3A) respectively, due to maximum current output of amplifiers and power supply. Not only that I.S.M.C controller can stabilize the system in this case, it enables to achieve the good performance with small overshoot and shorter settling time. We can see that the duration of t=0~0.2sec is levitation stage and the effect of rotational speed will be occurring from t=0.2sec, the motor/generator start to charge/discharge in rotational stage as well.

5 Conclusions

In this paper, the measurements of active and passive magnetic bearings with segmented Halbach magnetized array are analyzed, the configuration and winding scheme effectively enable to simplify the system into a linear system. Furthermore, the stability problem of magnetic bearings for a flywheel energy storage system has been formulated with I.S.M.C controller. The illustrative example reveals that controller parameters are adequately adjusted for achieve to stabilize the unstable rotor and the robustness of suppressing the external disturbances and model uncertainties, such as assembly errors, manufacturing errors, mass unbalance and sensor noise, are further work scope. Actually, the current amplifiers always have limited output, so regulation of controller parameters also is a way to decrease control effort. So far, the dynamic of motor is neglected in simulation, we will consider that effect into the simulation for more realistic in future. The fabrication and manufacturing of proposed flywheel battery prototype will be done in near future, and the experiment and development of driver of motor/generator are main work scope in next stage.

References

[1] B. Bolund, H. Bernhoff and M. Leijon, Flywheel energy and power storage systems, *Renewable and Sustainable Energy Reviews 11*, 2007, pp. 235-258

[2] J. G. Bitterly, Flywheel Technology Past, Present, and 21St Century Projections, IEEE AES Systems Magazine, 1998

[3] O.J. Fiske and M.R. Ricci, Third generation flywheels for high power electricity storage, *the 19th International Conference on Magnetically Levitated Systems and Linear Drives*, Germany, September 2006

[4] Cao, Jianrong and Chen, Quanshi, Decoupling control for a 5-DoF rotor supported by active magnetic bearings, *Sixth international Conference on Electrical Machines and Systems*, 9-11 Nov 2003

[5] Li, Qunming, Yin, Songduo, Wan, Liang, and Duan, Ji'an, Stability Analysis and Controller Design for a Magnetic Bearing with 5-Degree of Freedoms, *The Sixth World Congress on Intelligent Control and Automation*, 21-23 June 2006

[6] Rundell, A. E., Drakunov, S. V., and DeCarlo, R. A., A Sliding Mode Observer and Controller for Stabilization of Rotatinal Motion of a Vertical Shaft Magnetic Bearing, *IEEE Transactions on Control Systems Technology*, Vol. 4, pp.598-608, September 1996

[7] Schweitzer, G. Bleuler, H., and Traxler, A., *Active Magnetic Bearings*, Hochschleverlag AG an der ETH Zurich, 1994

[8] S. Jinji, R. Yuan and F. Jiancheng, Passive axial magnetic bearing with Halbach magnetized array in magnetically suspended control moment gyro application, *Journal of Magnetism and Magnetic Materials 323*, 2011, pp. 2103-2107

[9] Y.M. Choi, M.G. Lee, D.G. Gweon, and J. Jeong, A new magnetic bearing using Halbach magnet arrays for a magnetic levitation stage, *Review of scientific instruments 80*, 045106, 2009